

Lecture Notes in Engineering

Edited by C. A. Brebbia and S. A. Orszag

54

T. J. Mueller (Editor)

Low Reynolds Number Aerodynamics

Proceedings of the Conference
Notre Dame, Indiana, USA, 5–7 June 1989



Springer-Verlag

**A Comparison Between Boundary Layer Measurements
in a Laminar Separation Bubble Flow
and Linear Stability Theory Calculations**

P. LeBlanc, R. Blackwelder, R. Liebeck
Department of Aerospace Engineering
University of Southern California
Los Angeles, California 90089-1191 USA

Abstract

This research examines the details of the boundary layer flowfield from wind tunnel measurements of a two-dimensional Liebeck LA2573A airfoil over a range of Reynolds numbers from 235000 to 500000. In this range, a laminar separation bubble becomes significant in the boundary layer and provides a measurable contribution to the airfoil drag. Measurements include airfoil drag, mean and turbulent boundary layer velocity profiles, a calculation of integral parameters associated with these profiles, and energy spectra of the velocity signal inside the boundary layer. Evidence of the growth of boundary layer velocity fluctuations within a range of frequencies in the laminar separation and transition regions has been found in these spectral measurements. Results have shown that the peak frequencies measured in the velocity spectra for the instability region agree with the most amplified wave number and frequency scaling predicted by linear stability theory for these inflectional profiles. Additionally, the maximum measured growth rates at this peak frequency correlate with growth rates calculated from similarly shaped Falkner-Skan profiles at the corresponding frequency of maximum amplification. This agreement between experimental and theoretical peak frequencies and growth rates was confirmed for the range of Reynolds numbers and for airfoil incidence ranging from zero lift to stall.

Introduction

The primary goal of this research is a better understanding of the transitional instability mechanism which has a controlling effect on the extent of laminar separation bubbles occurring on airfoils operating at low chord Reynolds numbers, generally for $R_e < 10^6$. In this range, the local Reynolds number based on the boundary layer development is often insufficiently high for Tollmein-Schlichting (viscous type) instabilities to promote a natural transition before the laminar boundary layer reaches an adverse pressure gradient and is subject to separation. Once laminar separation has occurred, the resulting inflectional velocity profiles promote a more rapid amplification of boundary layer fluctuations which eventually reach transition levels. Laminar

separation is also associated with a significant increase in the boundary layer thickness. After transition, increased mixing promotes growth of the turbulent separated shear layer which eventually reattaches to the airfoil surface in cases where the divergence of the separated laminar layer from the surface has not exceeded some critical point.

Research has shown that decreases in R_c tend to delay the transition region within the bubble. These decreases have been correlated with a thicker turbulent boundary layer and additional drag penalty due to the separation bubble. Meanwhile, the addition of external forcing conditions such as the free stream turbulence [1], acoustic disturbances [2] [3] [4], or surface roughness [4] has been found to encourage earlier transition, resulting in a smaller bubble and reduced drag. Accordingly, the transition position within the bubble can be considered a primary factor in controlling the low Reynolds number boundary layer flowfield, and its prediction becomes critical to airfoil performance calculations.

Early attempts at transition prediction focused on correlations of local flow parameters and Reynolds numbers in the laminar bubble region [5], [6], [7]. Later work in conjunction with additional data has indicated the limited success of such correlations [8]. More recently, numerical calculation methods have been proposed for predicting low Reynolds number separation bubble flows [9], [4], [10]. These methods involve linear stability calculations to some extent in determining transition within the viscous / inviscid interaction schemes. The transition calculations generally assume an e^n transition criterion based on the stability of Falkner-Skan (β) reverse flow profile solutions which is described in detail by van Ingen and Boermans [4]. Considering the more promising results in predicting separation bubble flows and airfoil performance with these methods, an attempt is made in the present study to compare peak frequencies and the corresponding growth rates from measured boundary layer velocity fluctuations in the laminar bubble with the most amplified waves and corresponding growth rates predicted by linear stability theory. Such a comparison would attempt to verify the stability calculations which are implemented in the e^n transition method.

A correlation between experimental and theoretical results is made assuming the standard small amplitude wave-like disturbance in the linear stability formulation for theoretical boundary layer profiles. A viscous Orr-Sommerfeld calculation has been used to determine the stability of various theoretical (β) profiles. The wave number and frequency have been nondimensionalized by the local edge velocity and displacement thickness: $\bar{k} = (2\pi\delta^*)/\lambda$, $\bar{\omega} = (2\pi f\delta^*)/U_e$. For calculations assuming spatially growing waves ($\bar{\omega}_i = 0$), an example of growth rates $-\bar{k}_i$ is given by figure 1 for the Falkner-Skan reverse flow profile at $\beta = -0.14$ and $R_{\delta^*} = 10^3$. The disturbance energy profile at some position \bar{x} downstream of the point of neutral stability (\bar{x}_0) for a particular wave number may be written as

$$E_{\beta}(x, y) = u^2(x_0, y) \exp \left[-2 \int_{x_0}^{\bar{x}} \bar{k}_i d\bar{x} \right] \quad (1)$$

and the local dimensional energy growth rate follows as

$$\frac{d(\ln E_{\beta}/u^2)}{dx} = \frac{-2\bar{k}_i}{\delta^*} \quad (2)$$

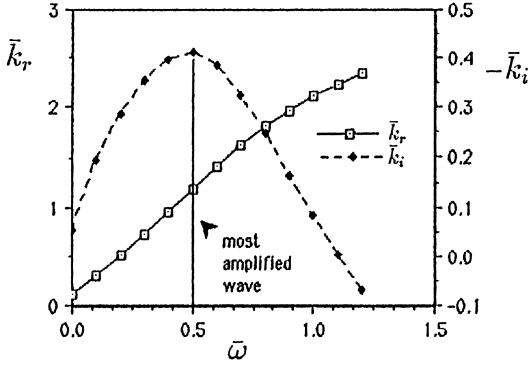


Figure 1: An example of typical growth rates for separated theoretical β profiles; $\beta = -.14$, $R_{\delta^*} = 1000$.

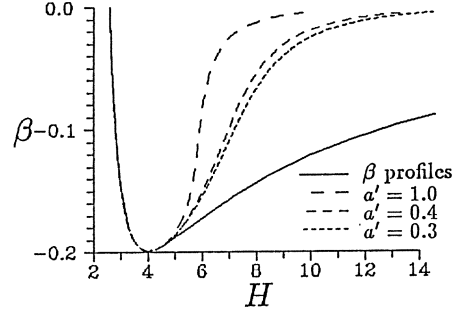


Figure 2: Falkner-Skan profile parameter β plotted against the profile shape factor H . Dashed curves represent rectified β profiles from eq. (3) for different a' .

This relation will be used in comparing calculated amplification rates with experimental data derived from boundary layer fluctuation energy spectra (E_s).

The subscript β in equation (2) refers to the pressure gradient parameter of the Falkner-Skan profiles which are used as an input to the stability calculation. These profiles are assumed for the separation bubble region in the numerical prediction schemes, and the shape factor H is essentially used as an independent variable since it uniquely describes both attached and separated profiles for decelerating flows ($-1.988 < \beta < 0$) as is indicated in figure 2. The β profiles may also be used to approximate measured mean velocity profiles upstream of transition. The shape factor H could then be used to associate experimental data with theoretical stability calculations. A problem arises, however, in the case of reverse flow profiles, where hot-wire anemometer velocity measurements cannot distinguish between velocity direction with respect to the flow sensor. The resulting experimental mean velocity profiles reflect a low magnitude rectified version of the separated profiles in the region near the wall. An example may be found in figure 3 which compares the $\beta = -.03$ reverse flow (solid line) profile with a profile measured in the separation region at $x/c = .385$, $\alpha = 4^\circ$ and $R_c = 235000$. Thus, while a theoretical reverse flow β profile could be matched to a particular experimental profile, (excluding the region of reverse flow), a calculation of the integral thickness parameters δ^* , θ and H would not indicate a match between the two shape factors. A solution to this problem is to modify the theoretical profile to simulate the experimental data in the reverse flow region strictly for the purpose of calculating δ^* , θ and H . A rectified theoretical profile is given by

$$\bar{u}_\beta^*(y) = \begin{cases} \bar{u}_\beta(y) & \bar{u}_\beta > 0 \\ a'|\bar{u}_\beta(y)| & \bar{u}_\beta < 0 \end{cases} \quad (3)$$

where an additional amplitude factor a' has been introduced to allow a better fit of the data. Two modified theoretical profiles ($a' = 1.0$ and $a' = 0.4$) are also compared with the experimental profile in figure 3. A reasonable match is indicated for an amplification factor of $a' = 0.4$;

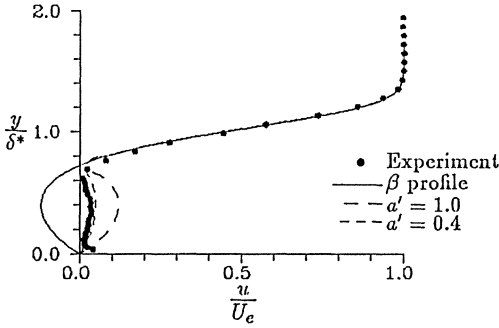


Figure 3: Comparison between typical separated experimental mean velocity profile ($R_c = 235000, \alpha = 4^\circ, x/c = .385$) and “matching” theoretical profile ($\beta = -.03$). Dashed curves represent rectified β profiles from eq. (3) for different a' .

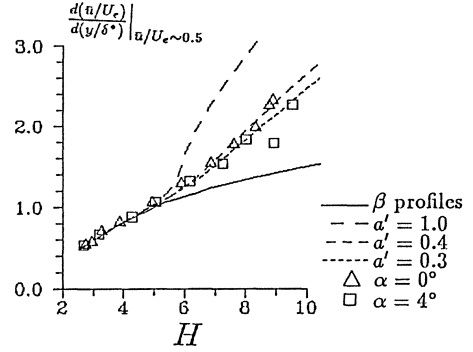


Figure 4: Nondimensional velocity shear near the profile inflection for theoretical (solid) and modified (dash) β profiles. Comparison is made with sample experimental data at $\alpha = 0^\circ, 4^\circ$ and $R_c = 235000$.

therefore, this value will be used in calculating a modified theoretical shape factor (H_β^*) for later comparisons with experimental results. This choice for a' is also supported by an examination of the nondimensional velocity shear ($d(\bar{u}/U_e)/d(y/\delta^*)|_{\bar{u}/U_e \sim 0.5}$) which has been approximated for the profile inflection. The theoretical curve in figure 4 for the case with $a' = 0.4$ shows a good representation of the sample data points at $\alpha = 0^\circ$ and 4° ($R_c = 235000$) over a range of profile shapes.

An estimate of the most amplified or peak frequency expected from experimental results can be made from the non-dimensional frequency scaling given above, with a few additional approximations. At a fixed airfoil incidence and chord position upstream of transition, the pressure distribution is assumed approximately constant; therefore, the profile shape, most unstable wave \bar{k}_r and convection speed \bar{c} (non-dimensional) can be approximated as constant over a range of R_c or for different chord lengths. In addition, if δ^* is approximated according to the Blasius relation $\delta^*/x \sim 1/\sqrt{R_x}$, then the frequency ratio should scale according to equation (4) for fixed chord, or equation (5) for fixed R_c .

$$\frac{f_{p1}}{f_{p2}} = \left(\frac{R_{c1}}{R_{c2}} \right)^{1.5} \Bigg|_c \quad (4)$$

$$\frac{f_{p1}}{f_{p2}} = \left(\frac{c_2}{c_1} \right)^2 \Bigg|_{R_c} \quad (5)$$

An estimate of experimental growth rates of spectral energy corresponding to peaks in the frequency spectra may be made by assuming an exponential growth of spectral energy in x . By differentiating spectral distributions with respect to the streamwise coordinate (x) at a fixed frequency f , and associating the result with equation (2), the experimental and theoretical

amplification rates can be compared by with the following relation

$$\bar{k}_i(\bar{\omega}) = \frac{-\delta^*}{2c} \frac{d(\ln \bar{E}_s)}{d(x/c)} \quad (6)$$

provided that the frequency ($\bar{\omega}$), local Reynolds number (R_{δ^*}) and profile shapes (H) have been matched. All terms on the right side of equation (6) are obtained from experimental data.

Alternatively, given the experimental spectral energy at a position corresponding to the maximum measured growth rate for the peak frequency (E_{s_0}), theoretical estimates for the spectral energy upstream of that position could be predicted by integrating the relation in (6) and using theoretical amplification rates as a function of profile shape:

$$E_s(x/c) = E_{s_0} \exp \left[2c \int_{x/c}^{(x/c)_0} \frac{\bar{k}_i}{\delta^*} d(x/c) \right] \quad (7)$$

This estimate would provide a check between values expected for the spectral energy and actual experimental values which could be associated with the signal noise level at a point sufficiently far upstream of the reference point.

Experimental Technique

Experimental measurements were conducted in the 37 by 54 inch semi-hexagonal cross section of the USC Dryden wind tunnel. This facility has a closed return with a contraction ratio of 7.1 and a maximum test section velocity of approximately 34 m/s. The free stream turbulence level in the test section has been measured at approximately .1% at airfoil test velocities for frequencies above 1 Hz.. Further details in reference [1] indicated that low frequency fluctuations on the order of 20 Hz. or less comprised a significant contribution to this turbulence.

Measurements were made on two LA2573A airfoil models designed by Liebeck [11] to operate at chord Reynolds numbers of approximately 250000. The airfoil contour is included in figures 7 and 9. Both 6 inch and 11.75 inch models were numerically milled from aluminum. In addition, the 6 inch chord model was equipped with pressure taps for lift measurements. Flowfield, pressure distribution and drag data were collected at $R_c = 235000$ (24 m/s) with the smaller model while the larger model was used to obtain flowfield and drag data at Reynolds numbers from 235000 to 500000. Drag measurements were calculated from the momentum deficit after a total pressure rake was centered in the airfoil wake. Boundary layer velocities were measured with a single hot-wire anemometer sensor, and the details of these measurements are given in [1].

Results / Discussion

Airfoil drag and boundary layer measurements were taken at Reynolds numbers of 235000, 300000, 375000 and 500000 for airfoil incidence ranging from $\alpha = -2^\circ$ to $\alpha = 12^\circ$ (near stall) in 2° increments. Measurements indicated that a separation bubble could still be found at $R_c = 500000$, except near stall. Boundary layer data on the airfoil lifting surface ranged in

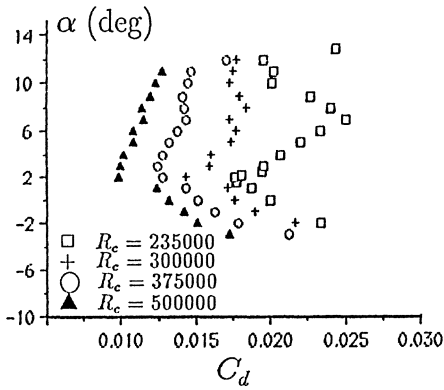


Figure 5: Experimental drag coefficients.

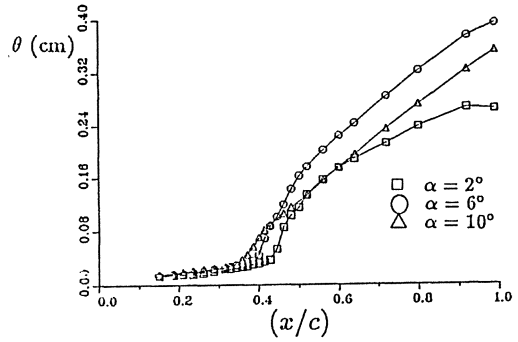


Figure 6: Boundary layer momentum thickness at $R_c = 235000$.

chord position from $x/c = .150$ to the trailing edge, including approximately 25 positions at each incidence with the highest concentration of data points located in the region of the laminar separation bubble. Boundary layer integral parameters δ^* , θ , H and δ_i were calculated directly from velocity profile measurements for all chord positions, including the separation region where the hot-wire measurement does not reflect the flow direction. Therefore, some error was introduced into these calculations using experimental data in the separation region. Brendel and Mueller [12] have estimated this error to be on the order of a few percent for δ^* while more significant for θ . Spectral measurements of the boundary layer velocity fluctuation were recorded at most profile data chord positions and were located at a distance normal to the surface corresponding approximately to the midpoint of the velocity shear layer (or approximately the maximum point in the velocity fluctuation ($\overline{u'}$) profile).

Airfoil Performance

Figure 5 illustrates the incremental drag penalty caused by the laminar separation bubble as R_c is reduced from 500000 to 235000 for airfoil incidence over the operating range. It can be seen that the penalty is more severe at midrange α for $R_c = 235000$ where the bubble is close to the point of bursting (failure of the turbulent separated shear layer to reattach). An examination of momentum thickness distribution in figure 6 shows that this drag penalty at lower R_c can be associated with the boundary layer growth downstream of the bubble. The case at $\alpha = 6^\circ$ shows the highest momentum thickness approaching the trailing edge, corresponding to the maximum drag for the three incidence cases plotted. Lower trailing edge values are found for θ at $\alpha = 10^\circ$ and $\alpha = 2^\circ$, which corresponds to their lower respective drag values. The airfoil lift has been measured for R_c in this range in [11] and [1] and does not show any significant sensitivity to bubble effects at these Reynolds numbers.

Boundary Layer Measurements

An example of experimental mean velocity profiles and mean fluctuation profiles measured with the 11.75 inch chord model are given in figure 7, for a Reynolds number of 235000 at $\alpha = 4^\circ$. The physical location of the measurement points are indicated on the airfoil in the upper right corner of figure 7. Profiles normalized with δ^* are plotted with increasing chord position from right to left and have been chosen to indicate the character of the boundary layer flowfield. The initial profiles at $x/c = .150$ and $.235$ show an attached boundary layer with a very low level in the (rms) fluctuation distribution. At $x/c = .287$, the inflectional profile nears separation. The following three normalized profiles at $x/c = .343$, $.371$, and $.399$ indicate a growing laminar separation region. (Measurements for δ^* in figure 8 illustrate that the separated laminar boundary layer region is in fact growing.) It can be seen that the hot-wire measurements fail to indicate reverse flow in the region near the wall, but do give an indication of the extent of this region. At $x/c = .427$, a jump in the magnitude of the mean fluctuation profile can be seen to indicate transition. Note that the large increase in the fluctuations does not occur near the wall as is often found in transition but corresponds to the location of the inflection point in the mean profile. A more precise definition of transition can be obtained by defining the "integral turbulence scale," $\delta_i^n(x)$, as

$$\delta_i^n(x) = \int_0^\delta \left(\frac{\overline{u'}}{U_e} \right)^n dy \quad (8)$$

This parameter is plotted for $n = 1$ at several R_c in figure 8. Transition can be clearly defined as the location where a sharp increase in this thickness parameter occurs. Finally, a reattached turbulent boundary layer can be found in figure 7 at $x/c = .520$. Profiles downstream of this position had a characteristic turbulent shape with normal growth in $\delta^*(x)$ and an approximately constant value of H . Note that $\delta_i^1(x)$ seems to increase proportionally with $\delta^*(x)$ in the reattached region.

In general, all boundary layer data where separation bubbles were found to occur showed the same general progression as that in figure 7, and this general character of the separation bubble flowfield has been measured by several other researchers [13], [12], [9], [4], [8], and [6]. At higher Reynolds numbers, normalized profiles have been found to match lower Reynolds number profiles quite well at the same nondimensional chord positions, except near transition which moves upstream with increasing Reynolds number. The experimental laminar and separated profiles in figure 7 are also compared with Falkner-Skan profiles. They generally correspond well at different x/c positions except in the reverse flow regions. Experimental shape factors in figure 8 were used to match the data with theory (H_β^*).

Spectral Measurements

Boundary layer velocity spectra associated with the profiles given in figure 7 are plotted in figure 9 at seven different chord positions extending through the separation bubble. It is noted that the chordwise progression proceeds from bottom to top, and that each curve has been

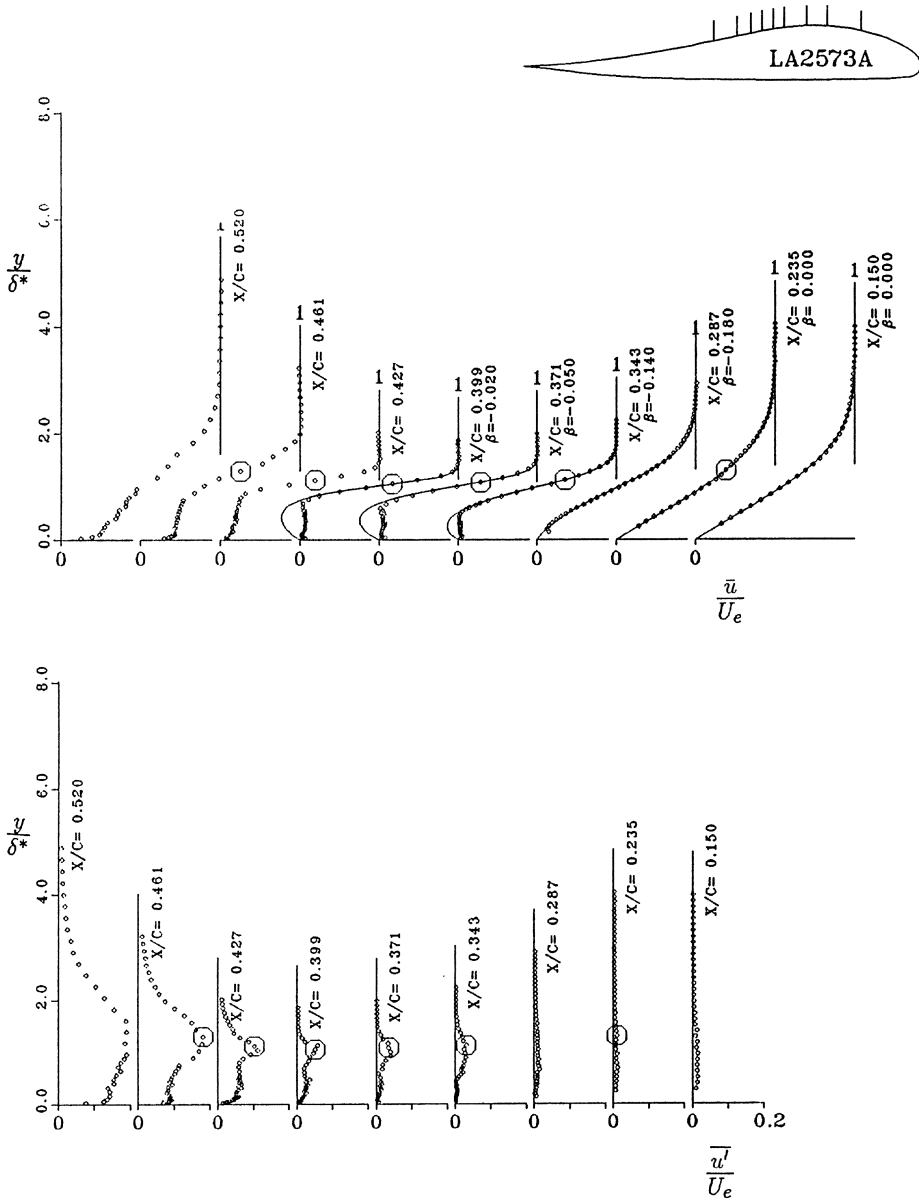


Figure 7: Mean and fluctuation velocity profiles at $\alpha = 4^\circ$, $R_c = 235000$. Symbols \odot indicate position at which spectral distributions in figure 9 were recorded. Solid curves show comparison with theoretical β profiles matched using the modified shape factor H_β^* .

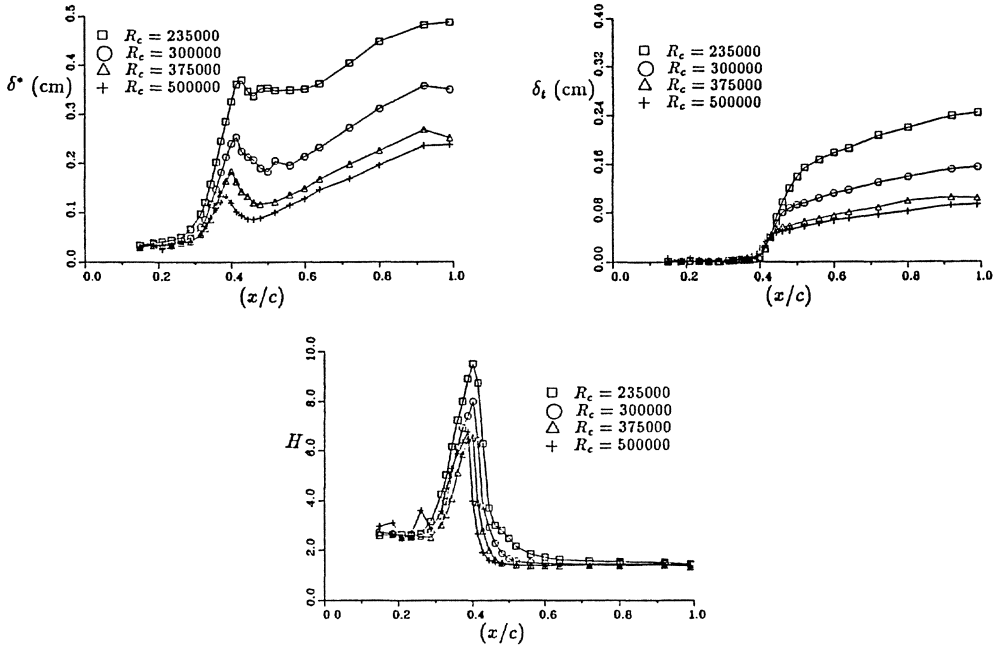


Figure 8: Integral thickness parameters δ^* , δ_t , and H at $\alpha = 4^\circ$.

offset from the previous curve by a distance of 1 decade. A distinct peak centered at 900 Hz. can be seen to grow from $x/c = .371$, at a point well into the laminar region of the bubble, to $x/c = .427$ where the peak seems to reach a maximum. This point also corresponds to the transition region as established in figures 7 and 8. At $x/c = .461$ the spectrum of a turbulent boundary layer velocity signal is observed.

Spectral distributions at higher Reynolds numbers and other airfoil incidence cases have shown the same general character as the data given in figure 9, with the exception that the peak is found to occur at a different frequency and over a different range of chord positions. In addition, similar boundary layer spectral progressions for separation bubble flowfields have been reported in [9], [12], [14], [1], and [3].

A comparison of peak frequency scaling with chord Reynolds number for different airfoil incidence cases is given in figure 10. The log-log plot indicates that peak frequencies follow a slope of approximately 1.5 which was anticipated from the stability theory formulation of equation (4). In addition, data at $R_c = 235000$ from the two different airfoil models confirmed the expected chord scaling for the frequency ratio in equation (5).

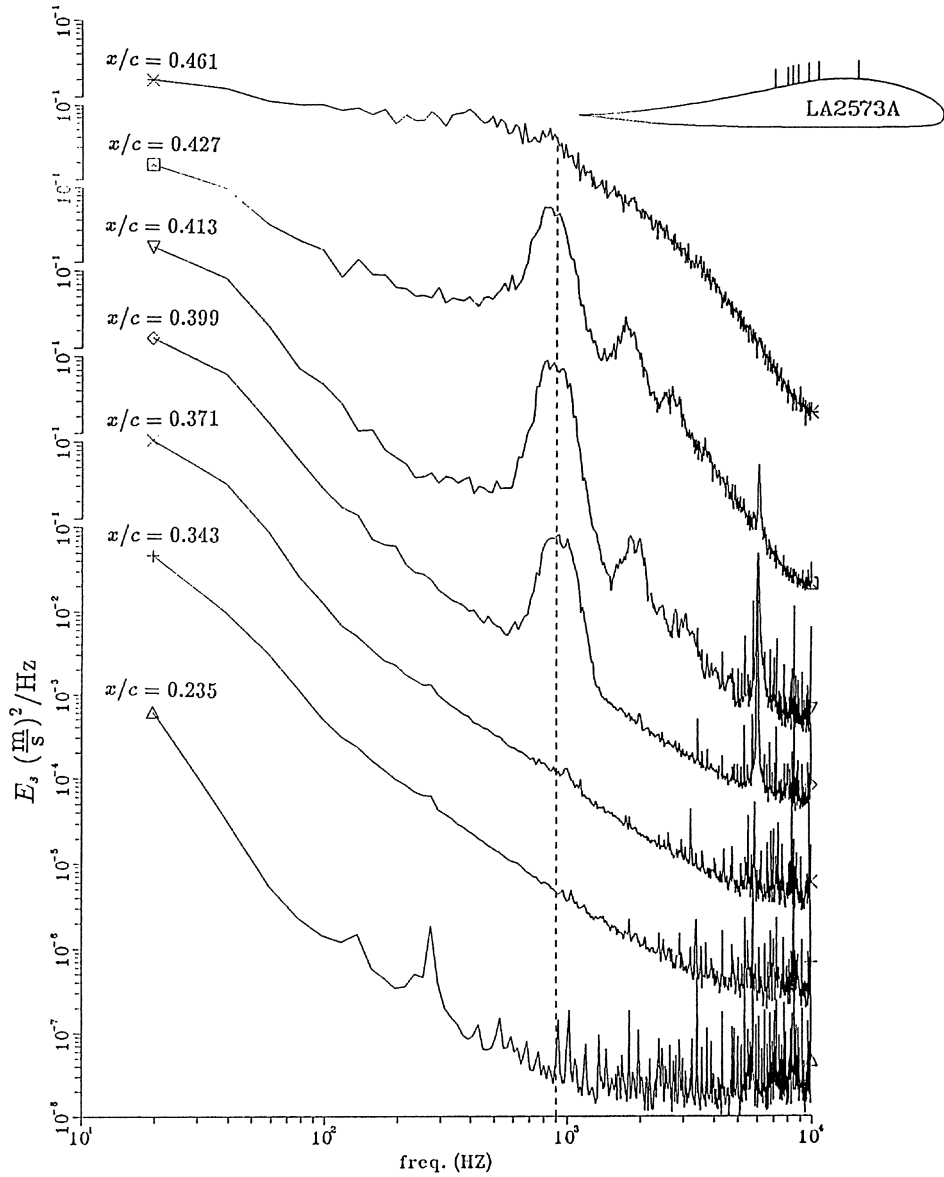


Figure 9: Boundary layer fluctuation spectral distributions for successive chord positions at $\alpha = 4^\circ$, $R_e = 235000$. Dashed line indicates instability peak growing at $f_p = 900$ Hz. Note: curves are vertically offset by 1 decade.

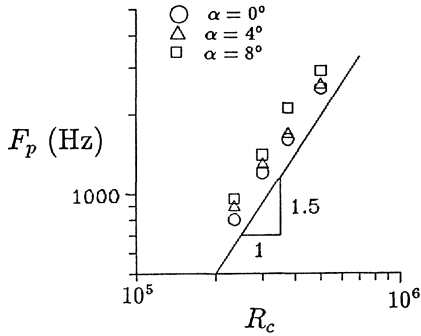


Figure 10: Scaling for peak frequency f_p with R_c .

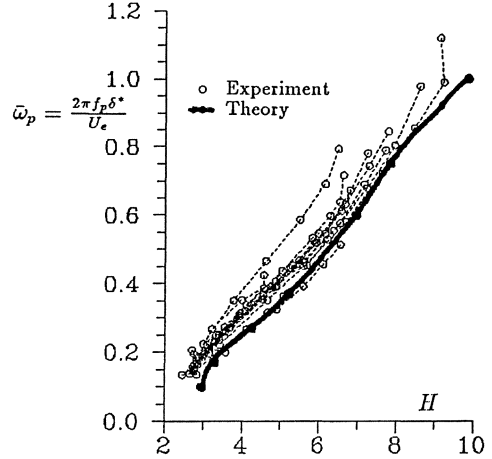
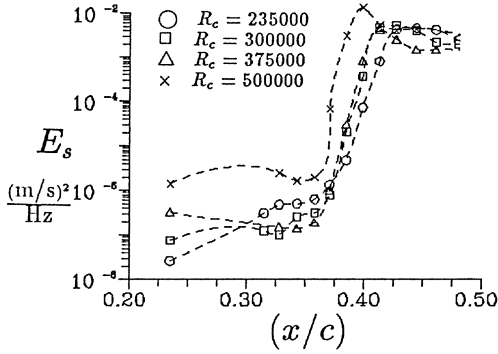
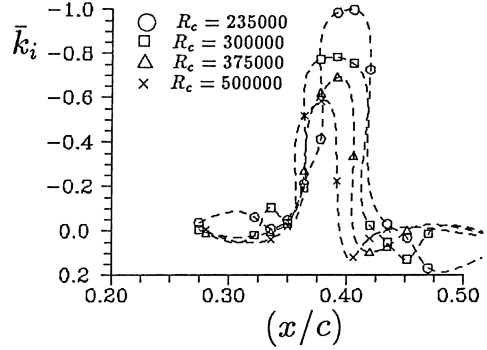


Figure 11: Correlation between $\bar{\omega}$ and profile shape H . Curves (o) include cases at $\alpha = 0^\circ, 4^\circ, 8^\circ, 10^\circ, 12^\circ$ and $R_c = 235000, 300000, 375000, 500000$. Comparison is made with theoretical values (•) assuming H_β^* .

Comparison With Stability Theory

For a comparison between the measured peak frequency and the most amplified waves expected from linear stability theory, the experimental peak frequency was non-dimensionalized as $\bar{\omega}_p = \frac{2\pi f_p \delta^*}{U_e}$ and plotted against the experimental shape factor in figure 11. It is noted that both δ^* and H are changing with the chordwise coordinate x in the region of the separation bubble; thus, an increase in H upstream of transition reflects a parameterized increase in x . The resulting curves represented by open symbols and dashed lines are given in figure 11 for a number of different Reynolds number and airfoil incidence cases ($235000 < R_c < 500000$, $\alpha = 0^\circ, 4^\circ, 8^\circ, 10^\circ, 12^\circ$). Curves are plotted for shape factors corresponding to x positions upstream of transition, and the rolloff at the upper end of each curve can be associated with the maximum in the H distribution found near transition (see figure 8 for example). In general, all curves tend to follow a straight line up until transition. These lines generally agree with the frequency corresponding to the most amplified wave for β profiles with varying shape factor. The theoretical peak frequencies are also given in figure 11 for $R_\delta^* = 2000$, and are designated by the solid symbols and line.

In order to provide a more complete comparison between experimental results and predictions estimated by linear stability theory, peak fluctuation growth rates will be examined for a variety of flowfield cases. The spectral energy at the peak frequency has been plotted against x in figure 12 for the Reynolds numbers investigated at $\alpha = 4^\circ$. This plot includes the values at $f_p = 900$ Hz. from figure 9. The curves show a sharp amplification just prior to transition, then the spectral energy generally levels off in the turbulent boundary layer region downstream. The

Figure 12: Spectral energy at f_p : $\alpha = 4^\circ$.Figure 13: Experimental growth rates (\bar{k}_i) at f_p : $\alpha = 4^\circ$.

maximum spectral energy occurs at a position just downstream of transition and the peak in the distribution for H in figure 8.

Using the relation from equation (6), non-dimensional growth rates can be calculated from the spectral energy curves of figure 12. These growth rates at f_p are given in figure 13 for the four R_c cases at $\alpha = 4^\circ$. The maximum growth rate for each curve is found to decrease and move upstream as Reynolds number is increased. The chord position of this maximum can be associated with the transition positions indicated by the jump in the δ_i distributions of figure 8.

For a comparison between experimental growth rates and theoretical estimates, the profile shape factor H must be substituted for the streamwise coordinate to provide a parameter with which to associate the two sets of results. This substitution may be associated with the use of H as an independant variable in the numerical flow prediction schemes such as [10]. Thus the experimental growth rates given in figure 13 have been replotted in terms of the experimental profile shape factor. The result in figure 14 also include growth rates at f_p for $\alpha = 0^\circ, 8^\circ, 10^\circ$, and 12° at the same chord Reynolds numbers as the $\alpha = 4^\circ$ data. The curve for each airfoil incidence and Reynolds number case is plotted from a profile shape corresponding to a chord position upstream of laminar separation, to the point of the maximum measured growth rate. Presumably, the data would be expected to follow a single trend in order to confirm the result predicted by linear stability theory. However, the experimental curves do not seem to collapse in general for the variety of flowfield cases included. The measured growth rates appear to be limited approximately by the dashed line indicated in figure 14. This line represents a best fit of the maximum measured growth rate for each case. This limiting relation is more clearly defined in figure 15 where these maximum measured growth rates are represented by open symbols. These maximum experimental amplification rates show a general agreement with the growth rates predicted by stability theory for the most amplified wave. The theoretical curve is given

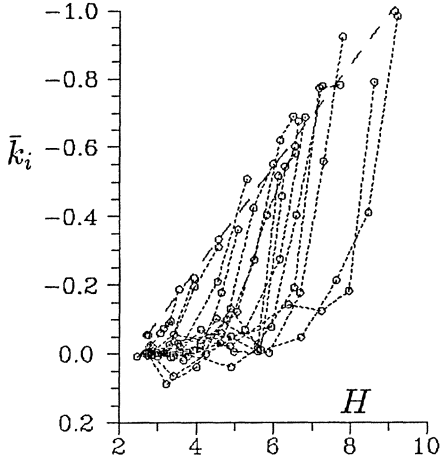


Figure 14: Correlation between experimental growth rates measured at f_p and profile shape. Curves (o) include cases at $\alpha = 0^\circ, 4^\circ, 8^\circ, 10^\circ, 12^\circ$ and $R_c = 235000, 300000, 375000, 500000$.

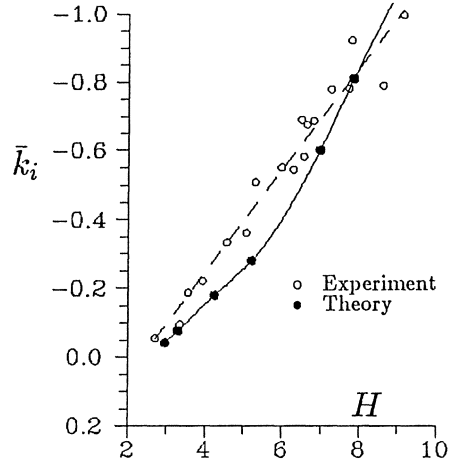


Figure 15: Correlation between maximum measured growth rates (o) in figure 14 at f_p and growth rates predicted by linear stability calculations (•) for profile shape factor H . (Theoretical values assume H_β^* .)

by the solid symbols for $R_s = 2000$.

One possible explanation for the disagreement between theoretical estimates and growth rates measured below the maximum for each case in figure 14 is the effect of the hot-wire velocity signal noise on the resolution of fluctuation amplitudes well below the maximum amplified values. A check of the expected spectral energy against the noise level may be made by extrapolating spectral energy levels at f_p upstream of the amplitude corresponding to the maximum measured growth rate. The extrapolation would use the relation given in equation (7) and assume that growth rates followed the theoretical curve in figure 15 in order to compare the amplitude of the spectral energy which would be expected upstream with the amplitudes actually measured. An example of this calculation is given in figure 16 in a format similar to that of figure 12. Two curves are plotted for the case $\alpha = 4^\circ$, $R_c = 235000$, using the spectral energy at $x/c = .406$ as a reference for the theoretical extrapolation. The experimental and predicted spectral energies agree for a short distance upstream of the reference point and then diverge as the experimental curve levels out. Thus, if this upstream level of the measured spectral energy were indicative of the signal noise level at the peak frequency, then the amplitude of fluctuations which would be expected below this noise level would be lost in the signal noise. The figure indicates that the actual spectral energy of fluctuations being amplified might only be resolved in measurements over a short region in x (or alternatively for a short variation in H .) Consequently, the comparison in figure 16 would infer that the disagreement found in figure 14 might be due to an experimental difficulty in the resolution of very low amplitude velocity fluctuations.

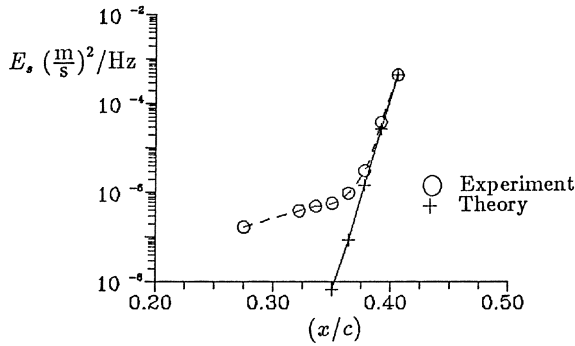


Figure 16: Comparison between measured and predicted spectral energy E_s at $\alpha = 4^\circ$, $R_c = 235000$. Data at $x/c = .406$ is used for theoretical extrapolation.

Conclusions

Comparisons between experimental boundary layer spectral fluctuation data for low Reynolds number separation bubble flows and linear stability theory calculations have shown that the peak frequency observed in the disturbance spectra corresponds to the most amplified waves predicted by theory for a large range of experimental conditions (R_c and α). These comparisons were made primarily for inflectional profile shapes in the separation region, leading to inflectional inviscid type instabilities, calculated with the Falkner-Skan profiles. In particular, measurements of f_p followed the predicted scaling for chord Reynolds number or chord variations. Comparisons between growth rates showed an agreement between the maximum experimentally measured growth rates at peak frequencies and predicted growth rates for the most amplified waves of similarly shaped profiles at a given airfoil incidence and Reynolds number. Discrepancies between measurements and theory at growth rates lower than the maximum were consistent with limitations in the resolution of the hot-wire velocity signal.

These results generally seem to show a favorable comparison between measurements upstream of the transition region and estimates predicted by linear stability theory associated with an inviscid inflectional profile. This agreement lends support to the use of linear stability theory calculations in determining the transition region for prediction methods designed to provide low Reynolds number laminar separation bubble flowfield calculations.

Acknowledgements

This work was supported by the Office of Naval Research under their University Research Initiative Contract N00014-86-K-0679 monitored by Mike Reischman. The authors would also like to thank P. Monkewitz for supplying the Orr-Sommerfeld code and S.-I. Chang for adapting it to our use.

Notation

a'	amplitude factor in eq. (3)
c	airfoil chord
\bar{c}	non-dimensional convection velocity $\bar{\omega}/\bar{k}_r$
C_d	airfoil drag coefficient per unit span $\frac{D}{Qc}$
D	airfoil drag
E_β	theoretical disturbance energy in eq. (1)
E_s	experimental spectral fluctuation energy (\bar{E}_s - nondimensional)
f	frequency
f_p	f corresponding to instability peak in E_s distribution
H	shape factor $\frac{\delta^*}{\theta}$
H_β^*	modified β profile shape factor (calculated with $\bar{u}^*(y)$)
\bar{k}	non-dimensional complex wave number $\bar{k}_r + i\bar{k}_i$
\bar{k}_r	non-dimensional wave number $\frac{2\pi\delta^*}{\lambda}$
\bar{k}_i	non-dimensional growth rate
L	airfoil lift
p	static pressure
Q	dynamic pressure $\frac{1}{2}\rho(U_\infty)^2$
R_c	Reynolds number, chord $(U_\infty c)/\nu$
R_{δ^*}	Reynolds number, displacement thickness $(U_e \delta^*)/\nu$
R_x	Reynolds number, local $(U_e x)/\nu$
u	time dependant streamwise velocity
\bar{u}, U	mean velocity $\frac{1}{N} [\sum_{j=0}^{N-1} u_j]$
u'	fluctuation velocity $u - \bar{u}$
\bar{u}'	mean fluctuation velocity $[\frac{1}{N} \sum_{j=0}^{N-1} (u_j - \bar{u})^2]^{1/2}$
\bar{u}_β^*	modified β profile mean velocity from eq. (3)
U_e	boundary layer edge velocity
U_∞	free stream velocity
x	chordwise position downstream of the airfoil leading edge
\bar{x}	non-dimensional distance x/δ^*
y	coordinate normal to the free stream or airfoil surface

Greek Symbols

α	airfoil angle of attack
----------	-------------------------

β	Falkner - Skan pressure gradient parameter
δ	boundary layer thickness
δ^*	displacement thickness $\int_0^\delta (1 - \frac{u}{U_e}) dy$
δ_t	"turbulence thickness scale" $\int_0^\delta (\frac{u'}{U_e}) dy$
θ	momentum thickness $\int_0^\delta \frac{u}{U_e} (1 - \frac{u}{U_e}) dy$
λ	disturbance wavelength
ν	kinematic viscosity
ρ	density
$\bar{\omega}$	non-dimensional frequency $(2\pi f \delta^*)/U_e$

References

- [1] P. J. LeBlanc, R. H. Liebeck, and R. Blackwelder. Boundary layer and performance characteristics from wind tunnel tests of a low Reynolds number Liebeck airfoil. In *Aerodynamics at Low Reynolds Numbers*, pages 8.1–8.19, London, Oct. 1986. The Royal Aeronautical Society.
- [2] K. B. Zaman, A. Bar-Sever, and S. M. Mangalam. Effect of acoustic excitation on the flow over a low-Re airfoil. *Journal of Fluid Mechanics*, 182:127–148, 1987.
- [3] C. F. Liu. *Control of Airfoil Performance by Local Excitation*. PhD thesis, National Cheng Kung University, Tainan, Taiwan, October 1988.
- [4] J. L. van Ingen and L. M. M. Boermans. Aerodynamics at low Reynolds numbers: A review of theoretical and experimental research at Delft University of Technology. In *Aerodynamics at Low Reynolds Numbers*, pages 1.1–1.40, London, Oct. 1986. The Royal Aeronautical Society.
- [5] D. E. Gault. An experimental investigation of regions of separated laminar flow. Technical report, NACA TN 3505, Sept. 1955.
- [6] M. Gaster. The structure and behavior of separation bubbles. Technical report, ARC R&M No. 3595, March 1967.
- [7] H. P. Horton. A semi-empirical theory for the growth and bursting of laminar separation bubbles. Technical report, ARC CP 1073, June 1967. (replaces ARC 29 185).
- [8] M. M. O'Meara and T. J. Mueller. Laminar separation bubble characteristics on an airfoil at low Reynolds numbers. *AIAA Journal*, 25(8):1033–1041, Aug. 1987.
- [9] C. Gleyzes, J. Cousteix, and J. L. Bonnet. Theoretical and experimental study of low Reynolds number transitional separation bubbles. In T. J. Mueller, editor, *Proceedings of*

the Conference on Low Reynolds Number Airfoil Aerodynamics, pages 137–152, University of Notre Dame, June 1985.

- [10] M. Drela and M. B. Giles. Viscous-inviscid analysis of transonic and low Reynolds number airfoils. Technical report, AIAA-86-1786, 1986.
- [11] R. H. Liebeck. Design and testing of an airfoil with positive pitching moment at low Reynolds numbers. Technical report, Douglas Aircraft Co., MDC 18893, Nov. 1982.
- [12] M. Brendel and T. J. Mueller. Boundary layer measurements on an airfoil at low Reynolds numbers. Technical report, AIAA-87-0495, 1987b.
- [13] M. Brendel and T. J. Mueller. Boundary layer measurements on an airfoil at a low Reynolds number in an oscillating free stream. Technical report, AIAA-87-1332, 1987a.
- [14] F. Hsiao, C. Liu, and Z. Tang. Experimental studies of airfoil performance and flow structures on a low Reynolds number airfoil. Technical report, AIAA-87-1267, 1987.